

Datasheet for 600-401-914S

Histone H2AvD phosphoS137 Antibody**Overview**

Description:	Anti-Histone H2AvD pS137 (RABBIT) Antibody - 600-401-914S
Item No.:	600-401-914S
Size:	25 µL
Applications:	ELISA, IHC, WB, ChIP, EM, IF, Multiplex
Reactivity:	D. melanogaster
Host Species:	Rabbit

Product Details

Background:	Variant histones H2A are synthesized throughout the cell cycle and are very different from classical S-phase regulated H2A. H2AvD is vital for viability, but the exact function of variant histones H2A is not known. H2A is a core component of the nucleosome, an octamer containing two molecules each of H2A, H2B, H3 and H4. The octamer wraps approximately 146 bp of DNA. HsAvD is expressed both maternally and zygotically and is found in embryos through to adults (female only). The human homologue, H2AX, is phosphorylated by ATM protein kinase when double strand DNA breaks occur. In mouse, H2AX "knock out" mice have an increased incidence of cancer.
Synonyms:	rabbit anti-H2AvD pS137 antibody, rabbit anti-Histone H2A.v pS137 antibody, H2AvD protein antibody, H2A.F/Z, H2A.Z, H2AvD, His2AvD, His2Av
Host Species:	Rabbit
Clonality:	Polyclonal
Format:	IgG

Target Details

Gene Name:	His2Av
Reactivity:	D. melanogaster
PTM Specificity:	Phosphorylation
Immunogen Type:	Conjugated Peptide

Immunogen:	Histone H2AvD pS137 Antibody was prepared from whole rabbit serum produced by repeated immunizations with a synthetic peptide corresponding to the C-Terminal region near amino acids 125-141 of <i>Drosophila melanogaster</i> (fruit fly) H2AvD protein.
Purity/Specificity:	This antibody is designed, produced, and validated as part of a collaboration between Rockland and the National Cancer Institute (NCI) and is suitable for Cancer, Immunology and Nuclear Signaling research. Variant histones H2A are synthesized throughout the cell cycle and are very different from classical S-phase regulated H2A. H2AvD is vital for viability, but the exact function of variant histones H2A is not known. H2A is a core component of the nucleosome, an octamer containing two molecules each of H2A, H2B, H3 and H4. The octamer wraps approximately 146 bp of DNA. HsAvD is expressed both maternally and zygotically and is found in embryos through to adults (female only). The human homologue, H2AX, is phosphorylated by ATM protein kinase when double strand DNA breaks occur. In mouse, H2AX "knock out" mice have an increased incidence of cancer.
Relevant Links:	<ul style="list-style-type: none">• NCBI - 17738227• UniProtKB - P08985• GenelD - 43229

Application Details

Tested Applications:	ELISA, IHC, WB
Suggested Applications:	ChIP, EM, IF, Multiplex (Based on references)
Application Note:	Histone H2AvD pS137 Antibody is tested in ELISA, Immunohistochemistry, and by western blot. Specific conditions for reactivity should be optimized by the end user. Expect a band approximately 14 kDa in size corresponding to phosphorylated H2AvD protein by western blotting in the appropriate <i>Drosophila</i> tissue or cell lysate or extract. Minimal reactivity is observed against the non-phosphorylated form of the immunizing peptide. This antibody is phospho specific for pS137 of H2AvD protein.
Assay Dilutions:	All assays should be optimized by the user. Recommended dilutions (if any) may be listed below.
ELISA:	1:4,000 - 1:20,000
IHC:	2 ug/ml
WB:	1:500 - 1:2,000

Formulation

Physical State:	Liquid (sterile filtered)
Concentration:	1.01 mg/mL by UV absorbance at 280 nm

Buffer: 0.02 M Potassium Phosphate, 0.15 M Sodium Chloride, pH 7.2

Preservative: 0.01% (w/v) Sodium Azide

Stabilizer: None

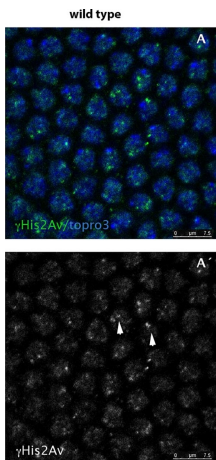
Shipping & Handling

Shipping Condition: Dry Ice

Storage Condition: Store vial at -20° C or below prior to opening. This vial contains a relatively low volume of reagent (25 µL). To minimize loss of volume dilute 1:10 by adding 225 µL of the buffer stated above directly to the vial. Recap, mix thoroughly and briefly centrifuge to collect the volume at the bottom of the vial. Use this intermediate dilution when calculating final dilutions as recommended below. Store the vial at -20°C or below after dilution. Avoid cycles of freezing and thawing.

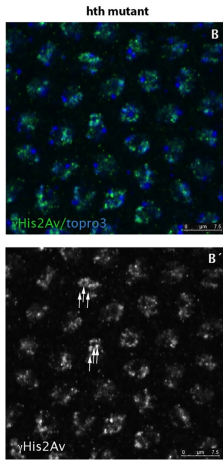
Expiration: Expiration date is one (1) year from date of receipt.

Images



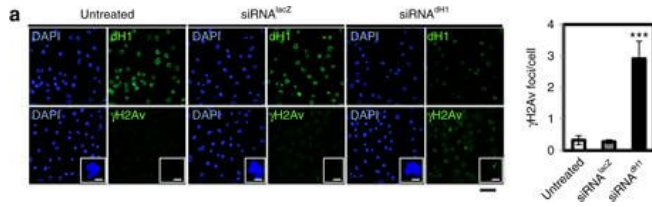
Immunofluorescence Microscopy

hth mutant nuclei show increased number of DNA breaks. A, A') Wild type syncytium (cycle 11) stained for His2AvP (green) and topo3 (blue). Due to the lack of mitotic checkpoints during the rapid syncytial divisions the nuclei show some degree of DNA breaks marked with the anti-His2AvP antibody (arrowheads in A'). B, B') However, hth mutant nuclei show more nuclear signal when stained with the same antibody (see arrows in B') indicating that they have more breaks in their DNA. C) Quantification of the DNA breaks in the Dfth mutant embryos and in their wild type siblings. Quantification was performed by counting the number of nuclear dots marked with the anti-His2AvP antibody. (N = 50 nuclei for each genotype from 5 different embryos each. P-value: 7,0085X10⁻⁵). Figure provided by CiteAb. Source: PLoS One, PMID: 25794008.



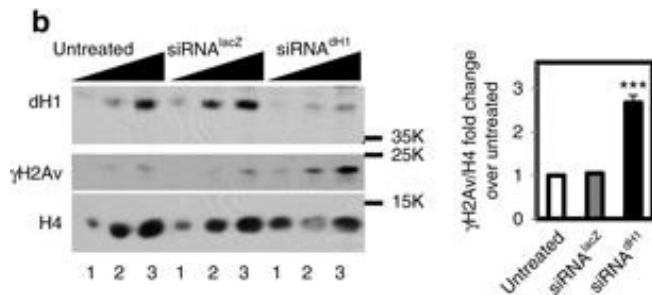
Immunofluorescence Microscopy

hth mutant nuclei show increased number of DNA breaks. A, A') Wild type syncytium (cycle 11) stained for His2AvP (green) and topo3 (blue). Due to the lack of mitotic checkpoints during the rapid syncytial divisions the nuclei show some degree of DNA breaks marked with the anti-His2AvP antibody (arrowheads in A'). B, B') However, hth mutant nuclei show more nuclear signal when stained with the same antibody (see arrows in B') indicating that they have more breaks in their DNA. C) Quantification of the DNA breaks in the Dfhth mutant embryos and in their wild type siblings. Quantification was performed by counting the number of nuclear dots marked with the anti-His2AvP antibody. (N = 50 nuclei for each genotype from 5 different embryos each. P-value: $7,0085 \times 10^{-5}$). Figure provided by CiteAb. Source: PLoS One, PMID: 25794008.



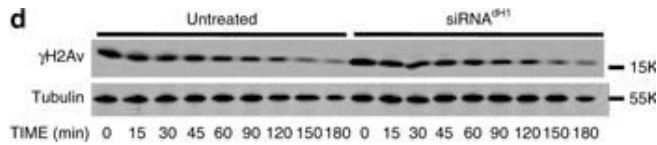
Immunocytochemistry

dH1 depletion induces DNA damage. a Immunostaining of dH1-depleted (siRNAdH1) and control undepleted cells (siRNALacZ and untreated) with αdH1 and αγH2Av antibodies (both in green). DNA was stained with DAPI (blue). Insets show enlarged images of representative individual cells. Scale bars are 20 μm and 2 μm in the Insets. On the right, the number of γH2Av foci per cell is presented (n > 100 for each condition). Error bars are s.e.m. The p-value of siRNAdH1 respect to siRNALacZ is indicated (***)p<0.005; two-tailed Student's t-test). b WB analyses with αdH1, αγH2Av and αH4 of increasing amounts of extracts (lanes 1–3) prepared from siRNAdH1, siRNALacZ and untreated cells. The positions corresponding to molecular weight markers are indicated. On the right, quantitative analysis of the results (N = 3). Error bars are s.e.m. The p-value of siRNAdH1 respect to siRNALacZ is indicated (***)<0.005; two-tailed Student's t-test). c Alkaline and neutral single-cell electrophoresis analyses of siRNAdH1, siRNALacZ and untreated cells. Scale bar corresponds to 20 μm. On the right, relative comet-tail moments are presented (n > 100 for each condition). Error bars are s.e.m. The p-values of siRNAdH1 respect to siRNALacZ are indicated (***)<0.005; two-tailed Student's t-test). d On the top, WB analysis with αγH2Av and αtubulin at different time points after X-ray irradiation (10 Gy) of siRNAdH1 and untreated cells. The positions corresponding to molecular weight markers are indicated. On the bottom, quantitative analysis of the results (N = 3) Figure provided by CiteAb. Source: Nat Commun, PMID: 28819201.



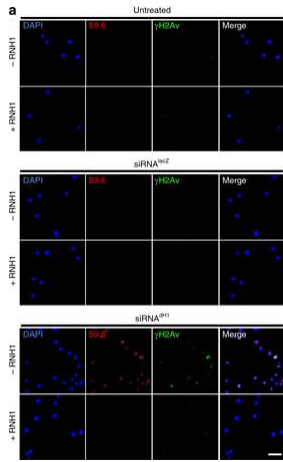
Western Blot

dH1 depletion induces DNA damage. a Immunostaining of dH1-depleted (siRNAdH1) and control undepleted cells (siRNAlacZ and untreated) with α dH1 and α γ H2Av antibodies (both in green). DNA was stained with DAPI (blue). Insets show enlarged images of representative individual cells. Scale bars are 20 μ m and 2 μ m in the Insets. On the right, the number of γ H2Av foci per cell is presented ($n > 100$ for each condition). Error bars are s.e.m. The p-value of siRNAdH1 respect to siRNAlacZ is indicated (***) $p < 0.005$; two-tailed Student's t-test). b WB analyses with α dH1, α γ H2Av and α H4 of increasing amounts of extracts (lanes 1–3) prepared from siRNAdH1, siRNAlacZ and untreated cells. The positions corresponding to molecular weight markers are indicated. On the right, quantitative analysis of the results ($N = 3$). Error bars are s.e.m. The p-value of siRNAdH1 respect to siRNAlacZ is indicated (***) < 0.005 ; two-tailed Student's t-test). c Alkaline and neutral single-cell electrophoresis analyses of siRNAdH1, siRNAlacZ and untreated cells. Scale bar corresponds to 20 μ m. On the right, relative comet-tail moments are presented ($n > 100$ for each condition). Error bars are s.e.m. The p-values of siRNAdH1 respect to siRNAlacZ are indicated (***) < 0.005 ; two-tailed Student's t-test). d On the top, WB analysis with α γ H2Av and α tubulin at different time points after X-ray irradiation (10 Gy) of siRNAdH1 and untreated cells. The positions corresponding to molecular weight markers are indicated. On the bottom, quantitative analysis of the results ($N = 3$) Figure provided by CiteAb. Source: Nat Commun, PMID: 28819201.



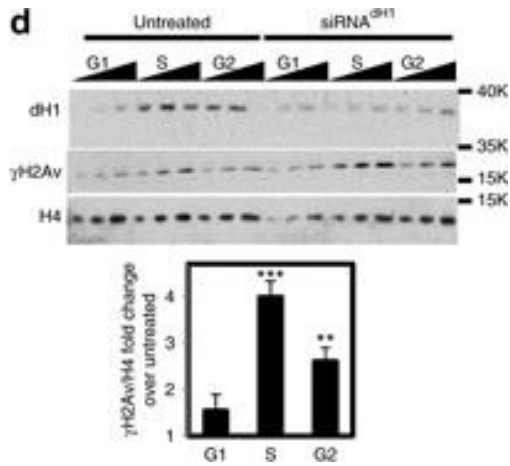
Western Blot

dh1 depletion induces DNA damage. a Immunostaining of dh1-depleted (siRNAdH1) and control undepleted cells (siRNAlacZ and untreated) with α dh1 and α γ H2Av antibodies (both in green). DNA was stained with DAPI (blue). Insets show enlarged images of representative individual cells. Scale bars are 20 μ m and 2 μ m in the Insets. On the right, the number of γ H2Av foci per cell is presented ($n > 100$ for each condition). Error bars are s.e.m. The p-value of siRNAdH1 respect to siRNAlacZ is indicated (** $p < 0.005$; two-tailed Student's t-test). b WB analyses with α dh1, α γ H2Av and α H4 of increasing amounts of extracts (lanes 1–3) prepared from siRNAdH1, siRNAlacZ and untreated cells. The positions corresponding to molecular weight markers are indicated. On the right, quantitative analysis of the results ($N = 3$). Error bars are s.e.m. The p-value of siRNAdH1 respect to siRNAlacZ is indicated (** $p < 0.005$; two-tailed Student's t-test). c Alkaline and neutral single-cell electrophoresis analyses of siRNAdH1, siRNAlacZ and untreated cells. Scale bar corresponds to 20 μ m. On the right, relative comet-tail moments are presented ($n > 100$ for each condition). Error bars are s.e.m. The p-values of siRNAdH1 respect to siRNAlacZ are indicated (** $p < 0.005$; two-tailed Student's t-test). d On the top, WB analysis with α γ H2Av and α tubulin at different time points after X-ray irradiation (10 Gy) of siRNAdH1 and untreated cells. The positions corresponding to molecular weight markers are indicated. On the bottom, quantitative analysis of the results ($N = 3$) Figure provided by CiteAb. Source: Nat Commun, PMID: 28819201.



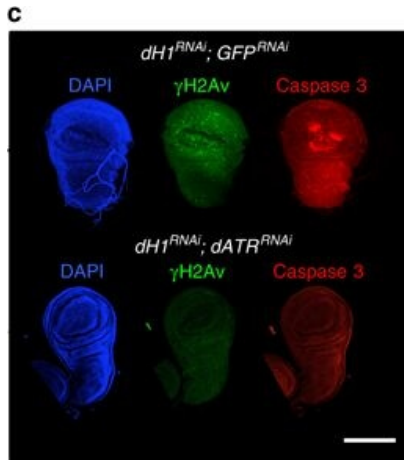
Immunocytochemistry

DNA damage induced by dH1 depletion associates with R-loops accumulation. a Immunostainings with $\alpha\gamma$ H2Av (green) and S9.6 (red) antibodies of siRNAdH1, siRNAlacZ and untreated cells overexpressing human RNH1 (+) or not (-). Scale bar corresponds to 10 μ m. b Quantitative analysis of the results shown in a. S9.6 (top) and γ H2Av (center) reactivities determined as the proportion of DAPI area stained with S9.6 antibodies and the number of γ H2Av foci per cell are presented ($n > 50$ for each condition). On the bottom, the extent of γ H2Av/S9.6 colocalization is presented as the proportion of γ H2Av area overlapping with S9.6 reactivity ($n > 50$ for each condition). Error bars are s.e.m. The p-values of siRNAdH1 respect to siRNAlacZ are indicated (no asterisk >0.05 , $***<0.005$; two-tailed Student's t-test). c $\alpha\gamma$ H2Av (top) and S9.6 (bottom) reactivities of G1-, S- and G2/M-phase sorted siRNAdH1, siRNAlacZ and untreated cells overexpressing RNH1 (+) or not (-) are presented as in b ($n > 50$ for each condition). Error bars are s.e.m. The p-values of siRNAdH1 respect to siRNAlacZ are indicated (no asterisk >0.05 , $***<0.005$; two-tailed Student's t-test). d WB analyses with α dH1, $\alpha\gamma$ H2Av and α H4 antibodies of siRNAdH1 and untreated cells sorted at G1-, S and G2/M-phase. The positions corresponding to molecular weight markers are indicated. Quantitative analysis is shown on the bottom ($N = 2$). Error bars are s.e.m. The p-values respect to untreated are indicated (no asterisk >0.05 , $**<0.01$, $***<0.005$; two-tailed Student's t-test) Figure provided by CiteAb. Source: Nat Commun, PMID: 28819201.



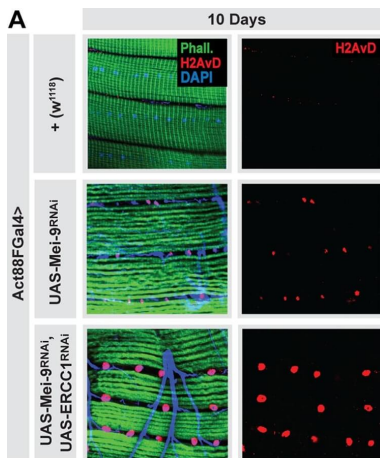
Western Blot

DNA damage induced by dH1 depletion associates with R-loops accumulation. a Immunostainings with $\alpha\gamma$ H2Av (green) and S9.6 (red) antibodies of siRNAdH1, siRNAlacZ and untreated cells overexpressing human RNH1 (+) or not (-). Scale bar corresponds to 10 μ m. b Quantitative analysis of the results shown in a. S9.6 (top) and γ H2Av (center) reactivities determined as the proportion of DAPI area stained with S9.6 antibodies and the number of γ H2Av foci per cell are presented ($n > 50$ for each condition). On the bottom, the extent of γ H2Av/S9.6 colocalization is presented as the proportion of γ H2Av area overlapping with S9.6 reactivity ($n > 50$ for each condition). Error bars are s.e.m. The p-values of siRNAdH1 respect to siRNAlacZ are indicated (no asterisk >0.05 , *** <0.005 ; two-tailed Student's t-test). c $\alpha\gamma$ H2Av (top) and S9.6 (bottom) reactivities of G1-, S- and G2/M-phase sorted siRNAdH1, siRNAlacZ and untreated cells overexpressing RNH1 (+) or not (-) are presented as in b ($n > 50$ for each condition). Error bars are s.e.m. The p-values of siRNAdH1 respect to siRNAlacZ are indicated (no asterisk >0.05 , *** <0.005 ; two-tailed Student's t-test). d WB analyses with α dH1, $\alpha\gamma$ H2Av and α H4 antibodies of siRNAdH1 and untreated cells sorted at G1-, S and G2/M-phase. The positions corresponding to molecular weight markers are indicated. Quantitative analysis is shown on the bottom ($N = 2$). Error bars are s.e.m. The p-values respect to untreated are indicated (no asterisk >0.05 , ** <0.01 , *** <0.005 ; two-tailed Student's t-test) Figure provided by CiteAb. Source: Nat Commun, PMID: 28819201.



Western Blot

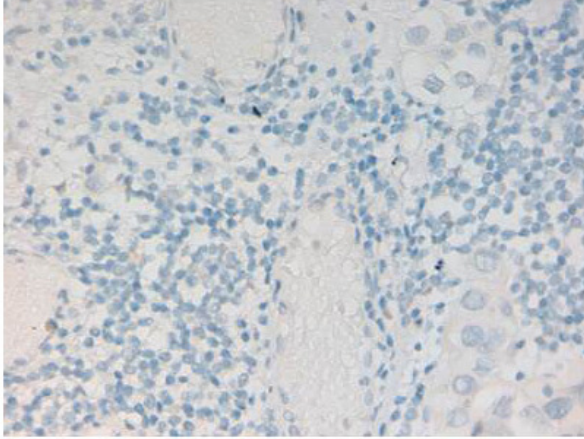
R-loops induced by dH1 depletion activate JNK-dependent apoptosis. a Wings from dH1-depleted his1RNAi flies of the indicated genotypes where dH1 depletion was induced in the pouch region of the wing imaginal disc. Scale bar corresponds to 500 μ m. b Quantitative analysis of the wing area of dH1-depleted his1RNAi flies of the indicated genotypes. Data is expressed as fold change respect to control dH1-depleted his1RNAi; GFP RNAi ($n > 20$ for each condition). Error bars are s.e.m. The p-values respect to control his1RNAi; GFP RNAi are indicated (** < 0.01 , *** < 0.005 ; two-tailed Student's t-test). c Immunostaining with α γH2Av (green) and α Caspase 3 (red) of wing imaginal discs from dH1-depleted his1RNAi flies upon dATR RNAi co-depletion (bottom) or not (top). DNA was stained with DAPI (blue). d Immunostaining with α Caspase 3 (red) of wing imaginal discs from dH1-depleted his1RNAi flies upon p53 RNAi co-depletion (bottom) or p53H159N overexpression (top). DNA was stained with DAPI (blue). e As in d but upon bsk RNAi co-depletion (top) or puc2A overexpression (bottom). Scale bars in c–e are 200 μ m. Figure provided by CiteAb. Source: Nat Commun, PMID: 28819201.



Immunofluorescence Microscopy

Systemic hormetic responses from muscle-specific DNA damage. (A) Detection of DNA damage (double strand breaks) in dissected longitudinal thoracic muscle of young (10 d) Act88FG4>+(w1118) controls, and flies with DNA repair attenuation specifically in thoracic muscle (mu-specific, Act88FG4>UAS-Mei-9RNAi or Act88FG4>UAS-Mei-9RNAi, UAS-ERCC1RNAi); assayed by phospho-H2aV immunostaining (red), counterstained with phalloidin ("Phall"; green, actin filaments) and DAPI (blue). Representative images shown. (B) Immunostaining to detect poly-ubiquitin protein (aggregates; "Poly-Ub.") in dissected longitudinal thoracic muscle from young (10 d) and old (30 d) flies, genotypes described above; anti-poly-ubiquitin (green), counterstained with phalloidin (red, actin filaments). Representative images shown. (C-D). Survival curves (lifespan, female flies) associated with mu-specific inhibition of Mei-9 using (C) the Act88FGal4 driver (compared to Act88FG4>+[w1118] controls) or (D) a GeneSwitch inducible driver (Act88FGS, +RU486 compared with -RU486 [vehicle alone] sibling controls). (E) Quantification of mitoses per whole dissected midgut

(assayed by anti-pH3 immunostaining) at indicated ages, genotypes described above; bars represent mean \pm SE, n = 25–30. (F) Immunostaining of dissected intestines to assess epithelial integrity of posterior midguts at indicated ages, genotypes described above; pH3 (green), armadillo (“Arm”; membrane, red), and DAPI (blue). Representative images shown. (G-H) Lineage tracing from ISCs using FRT recombination of a split alpha-tubulin-lacZ transgene (in Act88FG4>+[w1118, controls] or Act88FG4>UAS-Mei-9RNAi genetic background). (G) Changes in clone size (cell per clone from posterior midgut) at indicated ages; represented as box plot (median, red line), n = 25. (H) Representative images of lacZ clones from various genotypes at indicated ages, immunostaining of dissected midguts (posterior), anti-lacZ (green), and DAPI (blue). (I) Venn diagrams showing overlap of up-regulated genes (from dissected midguts) between Act88FG4>UAS-Mei-9RNAi and controls Act88FGal4>+(w1118) during aging (transcriptomes at 30 d, compared to Act88FGal4>+[w1118] controls at day 10). The threshold for genes included in the analysis was (i) changes in RPKM values of at least 2-fold up-regulated in intestine compared to young controls and (ii) a minimum RPKM value of 2. (J) Fold change (in intestinal transcriptome RPKM values; Day 30 Act88FG4>UAS-Mei-9RNAi/ Day 10 Act88FGal4>+[w1118] control [black bars] or Day 30 control/Day 10 control [gray bars]) of selected innate immune genes. Underlying data can be found in S1 Data. See also S1 and S2 Figs and S1 and S2 Tables. FRT, flippase recombination target; ISC, intestinal stem cell; pH3, phospho Histone H3; mu-specific, muscle-specific; RPKM, reads per kbp per million reads; RU486, mifepristone. Figure provided by CiteAb. Source: PLoS Biol, PMID: 30036358.

**Immunohistochemistry**

Immunohistochemistry with anti-Histone Antibody. Tissue: Human Bladder Cancer. Fixation: FFPE buffered formalin 10% conc. Ag Retrieval: HIER citrate buffer pH6 or HIER EDTA pH9. Primary antibody: 2 ug/ml at 2 hr. Secondary Ab: anti rabbit polymer HRP 20 ' RT.

**Western Blot**

Western blot using Rockland's affinity purified anti-histone H2AvD pS137 antibody shows detection of a band at ~15 kDa corresponding to phosphorylated H2AvD (lane 2 arrow-head). Lane 1: mock-irradiated *Drosophila melanogaster* (3rd instar) larvae brain WC lysate. Lane 2: 4000-RAD gamma irradiated *Drosophila melanogaster* (3rd instar) larvae brain WC lysate. Separated on by SDS-PAGE and transferred to nitrocellulose. After blocking the membrane was probed with the primary antibody diluted to 1:500. Washes and reaction with secondary antibody followed incubation. Use HRP conjugated Gt-a-Rabbit IgG [H&L] MX (p/n 611-103-122) and ECL for detection. Personal Communication. Yikang Rong, NIH, CCR, Bethesda, MD.

References

- Neophytou C et al. Aberrant enterocyte progenitor clustering as an early life biomarker of *Drosophila* aging. *iScience*. (2025)
- Na HJ et al. Integrated ecdysone and O-linked N-acetylglucosamine signaling coordinates intestinal stem cell proliferation in *Drosophila* midgut. *G3 (Bethesda)*. (2025)
- Watase GJ et al. RNA polymerase II-mediated rDNA transcription mediates rDNA copy number expansion in *Drosophila*. *PLoS Genet*. (2024)
- Pilesi E et al. Vitamin B6 deficiency cooperates with oncogenic Ras to induce malignant tumors in *Drosophila*. *Cell Death Dis*. (2024)
- Parrella P et al. Bleomycin reduces *Vairimorpha (Nosema) ceranae* infection in honey bees with some evident host toxicity. *Microbiol Spectr*. (2024)

- Chauvin SD et al. Inherited C-terminal TREX1 variants disrupt homology-directed repair to cause senescence and DNA damage phenotypes in Drosophila, mice, and humans. *Nat Commun.* (2024)
- Rye T et al. Nup153 is not required for anchoring heterochromatic DSBs to the nuclear periphery. *MicroPubl Biol.* (2024)
- Guo T et al. Impaired dNKAP function drives genome instability and tumorigenic growth in Drosophila epithelia. *J Mol Cell Biol.* (2024)
- Crucianelli C et al. Distinct signaling signatures drive compensatory proliferation via S-phase acceleration. *PLoS Genet.* (2023)
- Torre M et al. A Drosophila model relevant to chemotherapy-related cognitive impairment. *Sci Rep.* (2023)
- Chang YH et al. Endogenous retroviruses and TDP-43 proteinopathy form a sustaining feedback driving intercellular spread of Drosophila neurodegeneration. *Nat Commun.* (2023)
- Zhang Q et al. Phase separation of BuGZ regulates gut regeneration and aging through interaction with m6A regulators. *Nat Commun.* (2023)
- Fontana P et al. Serine ADP-ribosylation in Drosophila provides insights into the evolution of reversible ADP-ribosylation signalling. *Nat Commun.* (2023)
- Torre M et al. A Drosophila model relevant to chemotherapy-related cognitive impairment. *Sci Rep.* (2023)
- González-Marín B et al. ATM/Chk2 and ATR/Chk1 Pathways Respond to DNA Damage Induced by Movento® 240SC and Envidor® 240SC Keto-Enol Insecticides in the Germarium of Drosophila melanogaster. *Toxics.* (2023)
- Tu R et al. Gap junction-transported cAMP from the niche controls stem cell progeny differentiation. *Proc Natl Acad Sci U S A.* (2023)
- Munden, A et al. Identification of replication fork-associated proteins in Drosophila embryos and cultured cells using iPOND coupled to quantitative mass spectrometry. *Scientific Reports* (2022)
- Gemble, S et al. Genetic instability from a single S phase after whole-genome duplication. *Nature* (2022)
- Richards L et al. Nucleoporins facilitate ORC loading onto chromatin. *Cell Rep.* (2022)
- O'Neill RS et al. Traip controls mushroom body size by suppressing mitotic defects. *Development* (2022)
- Liu J et al. NMNAT promotes glioma growth through regulating post-translational modifications of P53 to inhibit apoptosis. *Elife.* (2021)
- Lattao R et al. Mauve/LYST limits fusion of lysosome-related organelles and promotes centrosomal recruitment of microtubule nucleating proteins. *Dev Cell.* (2021)
- Casale AM et al. Transposable element activation promotes neurodegeneration in a Drosophila model of Huntington's disease. *iScience* (2021)
- Hatkevich t et al. A pathway for error-free non-homologous end joining of resected meiotic double-strand breaks. *Nucleic Acids Res.* (2021)
- Tu R et al. Multiple Niche Compartments Orchestrate Stepwise Germline Stem Cell Progeny Differentiation. *Curr Biol.* (2021)
- Mascolo E et al. Pyridoxine/pyridoxamine 5'-phosphate oxidase (Sgll/PNPO) is important for DNA integrity and glucose homeostasis maintenance in Drosophila. *J Cell Biol.* (2020)

- Rastegari E et al. WD40 protein Wuho controls germline homeostasis via TRIM-NHL tumor suppressor Mei-p26 in *Drosophila*. *Development*. (2020)
- Palladino J et al. Targeted de novo centromere formation in *Drosophila* reveals plasticity and maintenance potential of CENP-A chromatin. *Dev Cell*. (2020)
- Na HJ et al. Nutrient-driven O-GlcNAcylation controls DNA damage repair signaling and stem/progenitor cell homeostasis. *Cell Rep*. (2020)
- Lin KY et al. Piwi reduction in the aged niche eliminates germline stem cells via Toll-GSK3 signaling. *Nat Commun*. (2020)
- Merigliano C et al. A new role for *Drosophila* Aurora-A in maintaining chromosome integrity. *Chromosoma*. (2019)
- Cosolo A et al. JNK-dependent cell cycle stalling in G2 promotes survival and senescence-like phenotypes in tissue stress. *Elife* (2019)
- Okumura K et al. Genetic identification and characterization of three genes that prevent accumulation of oxidative DNA damage in *Drosophila* adult tissues. *DNA Repair (Amst)*. (2019)
- [View More ...](#)

Disclaimer

This product is for research use only and is not intended for therapeutic or diagnostic applications. Please contact a technical service representative for more information. All products of animal origin manufactured by Rockland Immunochemicals are derived from starting materials of North American origin. Collection was performed in United States Department of Agriculture (USDA) inspected facilities and all materials have been inspected and certified to be free of disease and suitable for exportation. All properties listed are typical characteristics and are not specifications. All suggestions and data are offered in good faith but without guarantee as conditions and methods of use of our products are beyond our control. All claims must be made within 30 days following the date of delivery. The prospective user must determine the suitability of our materials before adopting them on a commercial scale. Suggested uses of our products are not recommendations to use our products in violation of any patent or as a license under any patent of Rockland Immunochemicals, Inc. If you require a commercial license to use this material and do not have one, then return this material, unopened to: Rockland Inc., P.O. BOX 5199, Limerick, Pennsylvania, USA.